ingegneria sismica
International Journal of Earthquake Engineering
Anno XLIII - Num. 2 - 2026

A Workbench-Based Study of Creep–Fatigue Coupling in Heat Transfer Tubes of Nuclear Power Steam Generators

Yiwei Chen[1], *Qiuhong Zhou*[1], *Hong Shi*[1], *Qiangsheng Zhang*[1] *and Dong Wei*[1,*]

[1] Nuclear and Radiation Safety Center, Ministry of Ecology and Environment, Beijing, 100082, China

SUMMARY: *In the present research, the Workbench software platform was taken as the core tool to carry deep exploration on the creep fatigue coupling problem which is encountered by the steam generator heat transfer tubes of nuclear power plants in the process of long-time operation. This research specially adopts simulation analysis methods to uncover the structure damage principle of heat transfer pipes under high-temperature high-pressure bad environments, which is produced by the together actions of material aging and circular stress. The research outcomes show that the present research is capable of forecasting the behavior properties of heat transfer pipes in practical running, therefore offering firm theoretical assistance for the secure running of nuclear power stations. Besides this, the research outcomes can offer scientific foundation for maintenance methods and life evaluation of connected equipment, hence help related workers to more correctly forecast and handle equipment performance, and hence guarantee the safety and high efficiency of nuclear power stations.*

KEYWORDS: *Evaporator heat transfer tube; High-temperature creep; Fatigue coupling; Aging; Workbench*

1 Introduction

As the core part of nuclear power steam generators, heat transfer pipes work without stop under super high-temperature and high-pressure situations, they are inevitably suffered from the combined actions of creep and fatigue [1, 2]. This research intends to clarify the creep-fatigue coupling behavior which is shown by heat transfer tubes in long-term operation, therefore providing a firm theoretical base and technical support for the safe running of nuclear power stations. The reciprocity between creep and fatigue speeds up the material failure processes, hence bringing bad influences upon the safety and reliability of the whole nuclear power station facilities. Hence, deep-going research on creep-fatigue interaction action is of great importance for the correct forecasting of working life, working out effective maintenance plans, and the optimization of design [3-5]. In the present research, we have massively made use of the high-level simulation software Workbench to establish the model for stress-strain situations of heat transfer pipes under real working conditions, hence comprehensively carrying out analysis on their creep-fatigue coupling action. These resultate give firm science basis for the amelioration of design and safety assessment of nuclear electricity steam generators.

To the heat-transfer pipe, the creep-fatigue coupling is controlled by three coupling variables: the part temperature field, the circle stress scope which comes from pressure and the vibration that flow brings, and the time-related creep strain that is accumulated when high

*dwei_nsc@126.com
https://doi.org/10.65102/is20261019
Published: 30 April, 2026

temperature is kept. One tube wall that has an outer diameter of 14 mm and a wall thickness of 1 mm possesses a small structural margin against local denting, formation of wear scars and initiation of cracks; Hence, the evaluation of damage cannot be carried out solely on the basis of the nominal membrane stress. The model which this paper puts forward uses the tube sheet, the head and the shell to be a whole constraint system, therefore the critical region it is expected that can appear in the place where thermal bending stress, pressure stress and restraint stress are superimposed together. The creep-fatigue life must be explained by a cumulative damage pattern, inside which the fatigue fraction $D_f = sum(n_i/N_i)$ is put together with the creep fraction $D_c = integral(dt/t_r)$. Under this framework, the lower peak stress which is got after relaxation does not mean the lower damage degree, because creep strain can keep on accumulating when stress gets reduction[16-18].

2 Establishment of the Finite Model

2.1 Geometric Parameters

The present research used a heat exchanger which has one-tube-pass and one-shell-pass structure, that is shown in Figure 1. For the purpose of studying the creep performance characters of these materials, the inlet temperature of the shell pass has been set to 490°C, hence the outlet temperature of the tube pass is kept at 370°C. In order to obtain a comprehensively understanding about the heat exchanger's size and constitution, the concerning geometry parameters are elaborately listed in Table 1. The head portion possesses an elliptical design that has a short-to-long axis proportion of 1:2, therefore it ensures structural symmetry and esthetic attraction. The thickness of the head part is in accordance with that of the shell main body, so that the whole structure strength and pressure-resistant ability can be kept [6, 7]. At one side of the head, the shell stretches out 10 mm past the tube sheet, which is a design that it has the function of promoting heat transfer efficiency and therefore it makes installation and maintenance become more convenient. The shell and the tube bundle usually are made by high-temperature resistance alloys, with surface processing methods like spiral grooves or fins being added to promote heat transfer effect. The regular doing of cleaning and inspection can significantly prolong the service life of the heat exchanger, and therefore guarantee the working efficiency of operation. In addition, this unit can be installed with pressure and temperature monitoring systems to carry out real-time working condition monitoring and ensure operation safety [8].

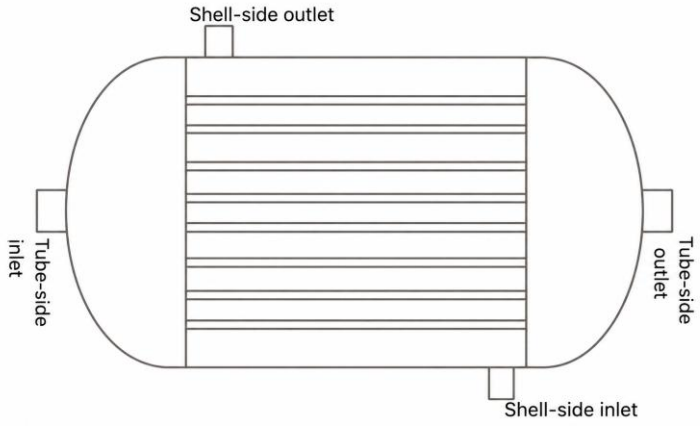

Figure 1: Schematic diagram of the heat exchanger structure

Table 1: Main dimensions of the heat exchanger (mm)

External diameter of the housing	thickness of shell	external diameter of the tube sheet	Plate tube thickness	External diameter of the heat exchange tube	Heat exchange tube thickness
159	4.5	159	12.5	14	1

The geometrical dimensions in Table 1 also define the pressure-stress scale used for the subsequent finite element interpretation. Using a thin-wall estimate, the shell hoop stress under 8 MPa is approximately pD/(2t) = 8 x 150/(2 x 4.5) = 133 MPa, whereas the heat-transfer tube hoop stress is approximately 8 x 12/(2 x 1) = 48 MPa. These values are below the reported maximum equivalent stress of 162.34 MPa, indicating that the peak stress is not produced by pressure alone. The additional stress component mainly comes from the head-cylinder transition, the tubesheet restraint and the temperature gradient through the perforated tubesheet. This also explains why the straight tube section does not become the maximum-stress location in the present calculation.

2.2 High-Temperature Model Simplification Process

To achieve a significant reduction in computation time and model complexity, this study neglected the inlet and outlet pipe sections during model construction. During the design phase, given the model's symmetrical characteristics, a quarter-scale model was selected as the subject of analysis. Additionally, the study assumes complete integration between the tubes and tube sheets, meaning their contact interactions were not incorporated into the model. To further minimize the number of elements and enhance computational efficiency, the minimum lengths of the shell and the portions of the heat exchange tubes extending beyond the tube sheet were determined using the edge effect formula. The edge effect formula is as follows:

$$L >= 2.5\sqrt{R\delta} \tag{1}$$

In the formula, the letter L represents the length affected by the edge effect δ δ; R denotes the inner radius of the heat transfer tube or shell, which corresponds to the wall thickness of the heat transfer tube or shell [9].

In the formula, the extension length $L_t \geq 6.12mm$ $L_t \geq 6.12mm$ of $L_s \geq 45.93$ the heat transfer $L_s \geq 45.93$ tube is, and that of the shell is. The length by which the heat pipe $L_1 = 35\text{mm}$ $L_s = 50\text{mm}$ shell protrudes beyond the tube $L_1 = 35\text{mm}$ $L_s = 50\text{mm}$ sheet must exceed the minimum extension length determined by the formula; therefore, in the model of this study, an additional value is adopted.

This formula, therefore, gives consideration to stress concentration events which are caused by temperature and pressure changes in the actual working process of heat exchangers, hence it ensures the accuracy and reliability of this model. When carrying out finite element analysis work, this research used high-precision grid division methods to ensure calculation accuracy. In addition, suitable boundary conditions and loads-including temperature fields, pressure fields, and possible mechanical loads-were put into the model to simulate the actual working conditions in reality. By means of these methods, this research therefore allows more accurate forecast of the heat exchanger's working effect under many kinds of working conditions.

The edge-effect cut short is tenable only when the axial stress and temperature gradients on the cut boundaries have decayed to a negligible degree. In this model, the truncation boundary

ought to be examined through comparing the equivalent stress on the artificial end surface with the stress in the neighboring full-thickness area. A discrepancy under 5% is a verification index that may be accepted for the simplified quarter model. Regarding the perforation region of the tubesheet, the dimension of elements ought to be controlled via the width of ligaments, instead of via the overall diameter of the shell. In the thin high-gradient layer, no less than three elements are needed for capturing the near-surface thermal stress; If not doing so, the computed maximum creep strain will be controlled by mesh insertion calculation and not by the material rule. The given mesh size with 96,705 nodes and 17,952 elements is sufficient for overall deformation, but the peak of creep strain must be verified through a partial mesh-independence comparison.

2.3 Physical Properties of High-Temperature Materials

The heat exchanger is built by 10GrMo910 steel, one material that is chosen for its outstanding physical properties, which as Table 2 shows in detail. This alloy structure steel is widely utilized in the making of heat exchange devices that work under high temperature and high pressure conditions. It not only possesses the quite good welding performance, but also has the high hot intensity and the anti-corrosive ability. The choice of this material is of great importance for guaranteeing equipment dependability and prolonging usage lifespan in the process of heat exchanger design and production.

Table 2: The Physics Characters of 10GrMo910 Steel Type

Temperature ${}^{0}C$	Room temperature	100	200	300	400	500
Modulus of *Pa* elasticity *Pa*	2.16×10^{11}	2.14×10^{11}	2.07×10^{11}	1.99×10^{11}	1.91×10^{11}	1.81×10^{11}
Poisson's ratio	0.3	0.3	0.3	0.3	0.3	0.3
Heat conductivity $W\cdot m^{-1}\cdot K^{-1}$	34.9	34	36.6	36.1	34.8	33.7
Coefficient K^{-1} of linear expansion K^{-1}	------	1.22×10^{-5}	1.25×10^{-5}	1.29×10^{-5}	1.33×10^{-5}	1.34×10^{-5}

The material sign that is used in the calculation corresponds to 10CrMo9-10/10CrMo910 Cr-Mo steel. Regarding this kind of steel, the modulus which depends on temperature, thermal conductivity and linear expansion coefficient are not secondary input parameters; they are the direct determinants of thermal bending behavior and stress relaxation process. Under the temperature of 490 °C, the decrease of modulus causes the reduction of instant stiffness, and the coefficient of thermal expansion thus increases the incompatibility that exists between the high-temperature shell-side layer and the lower-temperature tube-side area. Long-time working furthermore facilitates carbide grain growth and damage of cycle resistance, hence the fatigue behavior after high-temperature heat treatment can be different from the original state even when the maximum tensile strength has only a small change. Therefore, the creep-fatigue evaluation must use temperature-related material parameters for elasticity, creep and cyclic damage, hence not a room-temperature strength indicator.

2.4 Selection of the Metastasis Model

In the creep calculation process, we adopted the Modified Time Hardening model provided by the Workbench software. This model is particularly suitable for such applications.

The deformation behavior of simulation materials under long-term mechanical loading over time. Its core mathematical model accurately describes the hardening effects of materials across different time scales, thereby providing a scientific basis for engineering design and material selection.

$$\varepsilon_{cr} = C_1 \sigma^{C_2} t^{C_3+1} e^{\frac{-C_4}{(C_3+1)T}} \tag{2}$$

In the aforementioned $\sigma\,\sigma$ formula, σ denotes stress (in MPa), t represents C_1、C_2、C_3、C_4 C_1、C_2、C_3、C_4 $C_1 = 1.286\times10^{-12}$ $C_2 = 3.75$ $C_3 = -0.12$ $C_4 = 1596.76$ time, T denotes temperature, and α is $C_1 = 1.286\times10^{-12}$ a $C_2 = 3.75$ constant $C_3 = -0.12$ $C_4 = 1596.76$. According to relevant literature, the values of α, β, γ, and δ are specified in reference [12].

The time-hardening creep relation that is modified and used in Workbench ought to be utilized as a local strain-rate law instead of being used as a global displacement correction. As for every integration point, the increment of creep strain is ascertained by the current stress, the temperature and the increment of time, and the accumulated creep strain is hence fed back into the calculation of stress redistribution. This point has significance for the current heat exchanger, hence the maximum stress position after 1 hour is different from that after 10 hours. The curve of constant-stress creep may be utilized for the calibration of material constants, but the finite element analysis must, all the same, permit stress relaxation when there exists structural constraint. Hence the practical output is not merely the whole deformation; it is this pair of equal creep strain and released stress that is at the identical position. The damage index may be written as $D_c = integral_0^t dt/t_r$(sigma_eq,T), and the fatigue portion can be calculated from the local strain range which is got from the pressure-temperature cycle.

2.5 Finite Element Model

This research utilized hexahedral unit elements to carry out mesh division work. It is worth pointing out that, the tube-sheet area has gone through fine mesh refinement, in order to greatly promote computational precision in this key region. The meshed model that we obtain is shown in Figure 2, it includes 96,705 nodes and 17,952 elements, hence this kind of configuration can guarantee comprehensive and accurate data that are used for numerical analysis. In the process of finite element analysis, the quality of mesh directly decides both the accuracy and the efficiency of calculation results. Hence, besides the refinement work on the tube-sheet area, this research has carried out strict control on the whole grid quality. Through the optimization of mesh size and shape, uniformity and continuity in all areas of the model are kept, hence hence the calculation mistakes are made as small as possible. Furthermore, the independence checks of mesh have been carried out in order to verify computational accuracy, hence guaranteeing the stability and reliability of the results.

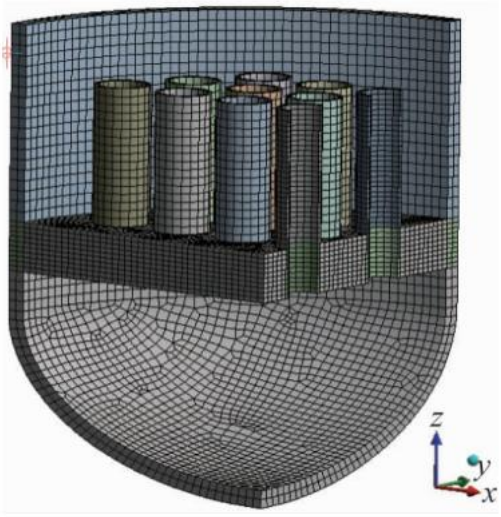

Figure 2: Finite Element Model of the Heat Exchanger

2.6 Analysis Methods and Boundary Load Studies

When we carry out the simulation analysis work, the most important task is to build a temperature field distribution model. This step is completed through utilizing the thermal analysis module which is inside the Workbench software. In the process of simulation, suitable boundary conditions were given: the shell side's inlet temperature was set as 490°C, and the tube side's outlet temperature was set as 370°C. In addition, for more accurate simulation of real work situations, adiabatic boundary conditions have been employed on the outer surfaces of the shell and the head, the shell end faces, and the two symmetric planes, for the purpose of stopping heat from losing in these areas. Through these collocation settings, we have gotten a precise temperature field distributing model.

After that, this research carried out an analysis of stress field by utilizing the structural analysis module of Workbench software. When we carry out the analysis of stress field, besides using the analysis results of temperature field obtained before, the special constraint conditions have been imposed on the heat exchange tubes and the end faces of cylinder. Concretely speaking, the displacement of these constituent parts along the z-direction was limited to zero, in order to simulate the fixed state they hold under real working situations. In addition, for the keeping of model symmetry, symmetric displacement restriction conditions were given onto the model's symmetry plane. By means of these arrangement methods, a precise stress field model has been gotten under the union functions of heat loads and inside heat exchanger pressure.

In the end, this research utilized a stress field model for the calculation of the creep deformation which is under the given stress conditions. In the work environment of heat exchange devices, long-term influences of temperature and pressure cause creep deformation to become a key element which affects equipment function and working life. Through the calculation of creep deformation, we are able to evaluate the working capability of the heat exchanger under real operation situations, and therefore make an estimation of its anticipated usage life span. In this simulation experiment, both the tube-side and shell-side working pressures were set to 8 MPa for copying normal working pressure situations, thus guaranteeing the accuracy and practical applicability of the obtained results.

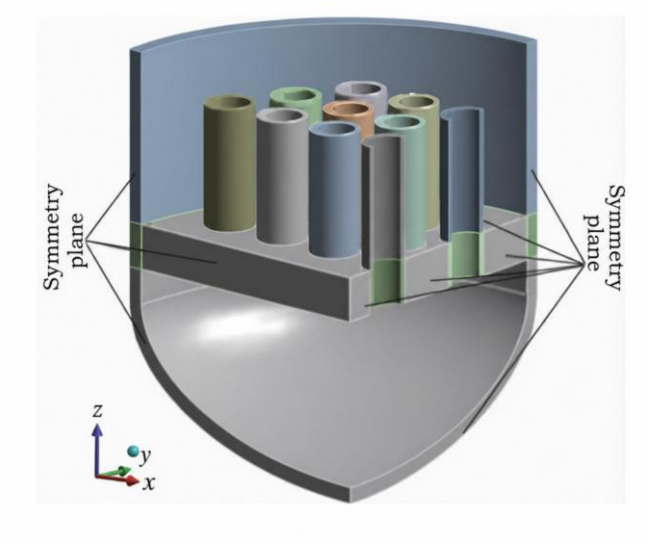

Figure 3: Schematic representation of boundary conditions

In the creep simulation process, the whole process is divided into two loading stages, in order to guarantee the accuracy and the efficiency. Firstly, the beginning loading stage must be as short as possible to exclude the impact of creep influences in the process of simulation. The time length of the second load stage is arranged to be 10 hours. In the initial periods of material action, creep strain velocities experience obvious changes; Hence, smaller initial time step augmentations are needed to catch these changes. To speak specifically, the beginning time step is set as 10-5 hours, which has a smallest time step of 10^-5 hours and a largest time step of 200 hours. In the course of this calculation stage, the creep selection must be turned on, and a creep limit proportion must be given to control the simulation precision of creep influences. According to related researches and experiences, the suggested value for the creep limit ratio normally has a scope from 1 to 10; In this simulation work, the author has set it as 1.

The boundary-load scheme that is shown in Figure 3 represents a problem that couples the thermal and structural fields, it is not two independent calculation processes. The consequence of heat gives the temperature gradient that passes through thickness, and this gradient, therefore, goes into the structure model as one externally given expansion field. Inner pressure gives a membrane constituent, while the limited expansion of the tubesheet and head brings bending and additional stress. The z-direction displacement restriction on tube and cylinder ends stops rigid-body movement and mimics axial restriction, hence it also adds extra stress close to the restricted area. This selection holds conservative property for the recognition of damage positions. The first loading step inhibits man-made creep in the process of load increasing, therefore the second step catches creep relaxation in the time of holding; The beginning time step of 10-5 h is suitable, because the early creep velocity changes more quickly than the later steady portion [15].

3 Simulation Results and Discussion

3.1 Temperature Field Simulation Results

Observation on data of Figure 4 clearly shows that, inside tube sheet tube-through area and along its thickness direction, temperature distribution of most regions closely accords with that of fluid on tube side of heat transfer tubes which leave tube sheet. This occurrence is mainly seen not including the extremely thin area that is next to the shell-side liquid, where temperature

values get close to those of the shell-side liquid. This distribution rule of temperature completely accords with the "epidermal effect" theory which is put forward by the American Society of Mechanical Engineers (ASME). Further analysis which uses Workbench software gives confirmation to this finding: inside the tube sheet hole-punching area, obvious temperature difference layers happen only in an extremely thin layer that is close to the tube sheet surface. This occurrence, which people usually call the "epidermal effect", is used to describe temperature changes that are near material surfaces and are caused by heat conduction.

Furthermore, this temperature distribution feature gives very important instruction for tube sheet design and material choice. In the process of carrying out design, engineers must have consideration for this temperature gradient to guarantee that thermal stresses inside the materials do not go beyond their allowable limits, hence thus preventing possible structural damage. In addition, the choice of suitable materials is of great importance, because different materials show different thermal conductivity values and thermal expansion coefficients-these factors together affect both the evenness of temperature distribution and the total thermal efficiency.

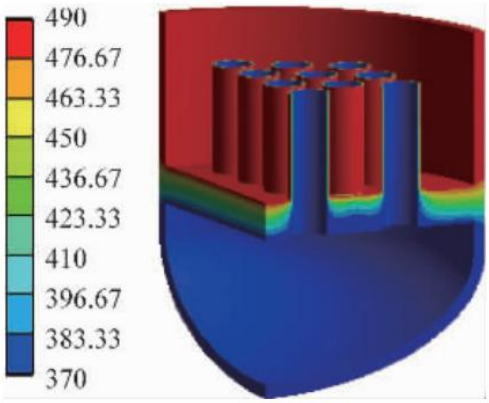

Figure 4: The stable state temperature distribution graph of the heat exchanging device (unit: degree Celsius)

The temperature shape line in Figure 4 displays that the region with holed tubesheet follows the temperature of tube-side exit through most of the thickness, hence the surface layer of shell-side draws near to the 490 °C boundary. This distribution brings about a bending-style heat load: the surface with higher temperature has the tendency to expand more than the inner part with lower temperature, but the adjacent shell, tubesheet and tubes put restrictions on the free expansion. The stress which we get is focused in the area where the head, shell and tubesheet rigidities are not continuous. This result accords with the stress field which has been reported, for the reason that the maximum equivalent stress does not solely appear at the boundary of the hottest fluid; it can be found at the place where the high-temperature layer has the mechanical restriction. For the explanation of creep-fatigue, the temperature gradient hence is more important than the absolute maximum temperature when confirming the damage high-risk area [16, 17].

3.2 Stress Field Simulation Results

Figure 5 very clearly shows that after one hour of working, the maximum equal stress in the heat exchanger arrived at 162.34 MPa, it is positioned on the inner side of the head that is near the connecting region with the cylinder. Until the 10-hour time point, the maximum equivalent stress has decreased to 139.44 MPa, its position having moved to the outer side of the head top.

This phenomenon shows that material creep deformation with the passage of time causes stress relaxation, therefore leading to the decrease of maximum equivalent stress numerical values and the corresponding position change of stress concentration points. More deep analysis makes it clear that this kind of stress relaxation has a very big influence on the long-time work stability of the heat exchange device. In the stages of design and material choice, the creep properties of materials must be taken into consideration, thus to guarantee safe and steady running in the whole expected working life period. In addition, the optimization of structural design-for instance, the modification of the connection mode between the head and the cylinder-can further lower the stress concentration, therefore it promotes the overall performance and service life of the equipment.

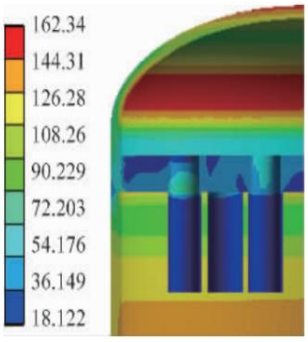

Figure 5: Equalizing stress distribution drawing of the heat exchanging device after one hour (MPa)

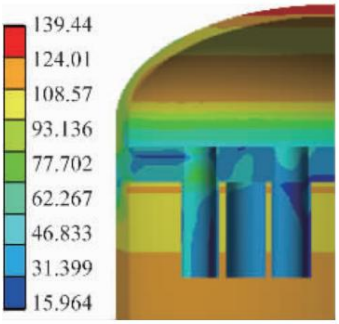

Figure 6: The equivalent stress distribution contour figure (MPa) of the heat exchanger which has worked 10 hours

The results of equivalent stress provide a quantitative indicator of stress relaxation. The maximum stress gets a decrease from 162.34 MPa when 1 hour passes to 139.44 MPa when 10 hours pass, which corresponds to a reduction of 22.90 MPa or 14.10%. Such kind of decrease is the usual situation of creep relaxation when displacement is restrained: a portion of the starting elastic strain gets changed into creep strain, therefore the local stress carries out redistribution toward neighboring areas. The movement of the biggest-stress place from the inside head-cylinder link to the outside head top shows that the head is the leading flexibility part in the holding process. To a pressure-boundary part, this peak numerical value should be divided into membrane, bending and local peak constituent parts. The membrane and membrane-add-bending parts have relation to pressure integrity, while the local peak part has relation to fatigue crack starting and creep strain accumulation.

3.3 Creep Deformation Simulation Results

Through careful examination of Figure 7 and Figure 8, we can clearly see that the total deformation quantity of the heat exchanger still keeps relatively small after the passing of one hour. To speak specifically, the maximum deformation occurrence is at the top position of the seal. Till 10 hours, the maximum deformation has risen to 40 millimeters, and this peak is still situated at the top of the seal. Furthermore, obvious deformation can be seen in the middle part of the cylinder, whose value gets close to that at the top of the seal. The comparison between the two figures shows that the locations of maximum deformation and minimum deformation still basically do not have change. It is worth pointing out that the deformation on the connecting surface between tube sheet and cylinder always keeps at a low level, hence it proves that the tube sheet effectively reduces the partial creep deformation in the connected cylinder segment.

The deeper study of Figure 7 and Figure 8 makes us discover that the deformation of the heat exchanger has a pattern which can be seen along with the change of time. In the one-hour observation process, though the deformation on the top of the seal was very small, it has already shown a possible trend of deformation. Until the 10-hour time point, the shape change at this position had a great increase to 40 millimeters - this increase is what shows that big damage has happened to the structure's stable ability under long-time working situations. At the same time, very big shape change was found in the central part of the round column, it can probably be blamed on the nature of the material, the design of the structure, and the environmental conditions of temperature and pressure. It ought to be pointed out that, although there exist very big shape changes in both the middle part of the cylinder and the upper part of the seal, the deformation that occurs at the connecting face between tube sheet and cylinder still keeps comparatively small. This further makes clear the very important function of the tube sheet in structural design: it not only keeps its own structural completeness but also effectively assigns stresses and reduces partial shape change in the cylinder.

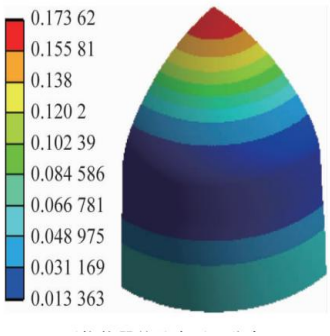

Figure 7: Cloud picture that displays the total distortion distribution of the heat exchanger when one hour has passed (mm)

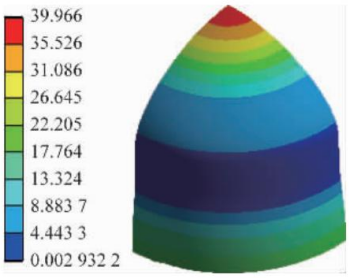

Figure 8: Cloud-shaped picture that displays the entire deformation distribution situation of the heat exchanger when 10 hours have passed (mm)

Through a meticulous checking of Figures 9 and 10, we can clearly see that after the passing of one hour, the maximum creep strain has appeared on the inner face of the head near the connecting position between the cylinder and the head, its strain size being 10^-5. This shows that no obvious creep event took place within this time interval. Nevertheless, when the time was prolonged to 10 hours, the circumstance altered greatly: the maximal creep strain rose obviously to 0.337, and this peak takes place in the area that is between the top of the head and the middle part of the cylinder. At the same time, the creep deformation quantities in the tube plate and heat exchanging tubes are comparatively low. The size and exact positions of the largest creep deformation match very closely with those that were before reported in the published works about creep deformation and failure appearance, therefore further proving the correctness and dependability of our simulation outcomes.

Furthermore, the comparison analysis made it clear that the distribution form of creep strain has a detectable rule with the passing of time. In the beginning stage, creep strain is mainly gathered in places where stress gathers, such as the connect place between the head and the cylinder body. Along with time going forward, the creep strain slowly extends to the middle area of the cylinder, this thus may have connection with material stress relaxation and the structural deformation ability. It is worth pointing out that, although creep strain has increase in some regions, the whole structure stability still has no obvious change, this shows that the materials and structure arrangement which are used in the design have very good creep resistance ability.

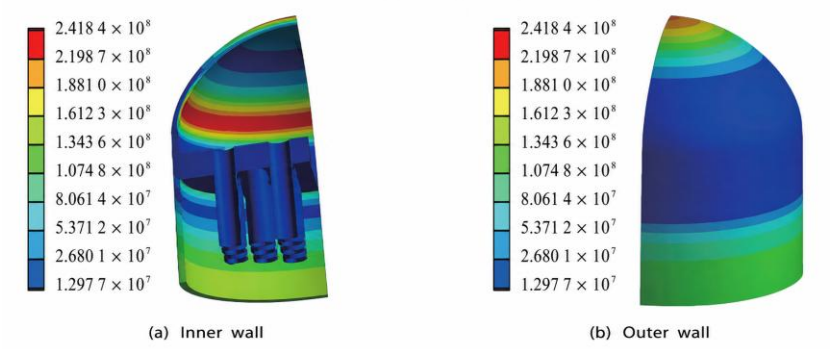

Figure 9: The cloud picture of equal creep strain distribution (MPa) from different viewing angles of the heat exchanger after 1 hour

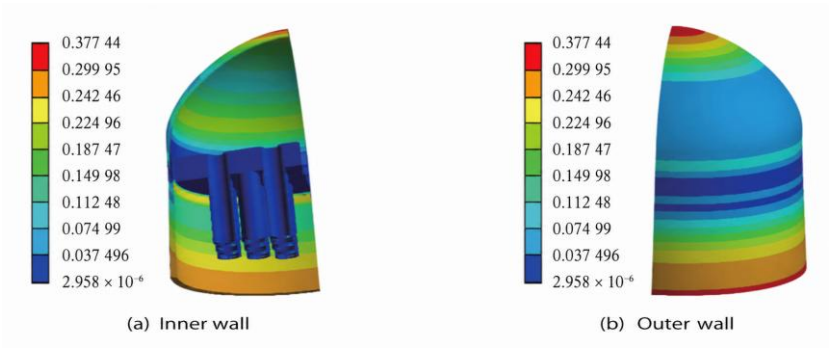

Figure 10: Cloud picture of equal creep strain distribution (MPa) from different viewing angles of the heat exchanger after 10 working hours

The deformation and creep-strain distribution pictures in Figures 7-10 display that the tubesheet area restrains radial distortion of the neighboring shell, while the head and middle shell part offer the main deformation ability. The 40 mm biggest deformation is big when

compared with the 159 mm outer diameter of shell, hence this result ought to be explained as a serious part creep-deformation situation instead of a small-deflection elastic reaction. The maximum equivalent creep strain which increases from about 10^-5 after 1 hour to 0.337 after 10 hours, this confirms that creep damage has very strong time-dependent property during the holding process. A strain magnitude of 0.337 also shows that the local damage condition is dominated by nonlinear strain accumulation; The decrease of pressure alone cannot be employed as a safe boundary. When we take the material's rupture strain as epsilon_r, a normalized creep strain ratio eta = epsilon_cr/epsilon_r may be utilized for comparing different operation cases and for defining inspection priority of the head top and shell middle region [20-25].

For life assessment, the simulation results identify two inspection-priority zones. The first is the head-cylinder transition, where the initial peak stress of 162.34 MPa appears and fatigue crack initiation is most likely during repeated start-up and shutdown cycles. The second is the head top and middle shell region, where the 10 h creep strain peak reaches 0.337 and the deformation reaches 40 mm. These two regions represent different damage modes: stress-driven fatigue at the transition zone and strain-driven creep at the head/shell deformation zone. The tubesheet and heat-transfer tubes show lower creep strain in the present model, but their safety margin should still be evaluated through local ligament stress and tube-wall thinning, because fretting, corrosion fatigue and foreign-object damage can reduce the fatigue limit independently of the global creep field.

4 Conclusion

(1) Utilizing finite element simulation technology, this study successfully elucidated the temperature field distribution characteristics of the heat exchanger under actual operating conditions. The findings revealed that in the tube sheet tube arrangement region, across most areas along the tube sheet thickness direction, the temperature closely matches that of the fluid in the tube side of the heat transfer tubes exiting the tube sheet. However, near the shell-side fluid, a thin layer exhibiting a pronounced temperature gradient was observed, with its temperature closely resembling that of the shell-side fluid.

(2) Further simulation analyses have discovered that after 10 hours of working, the maximum equivalent stress of the heat exchanger has a reduction compared with that tested after 1 hour of working, and the position of stress concentration also has a change in location. This occurrence is mainly ascribed to the stress releasing effect that is caused by material creeping distortion.

(3) In the simulation analysis that is carried out on the heat exchanger, serious creep phenomena were mainly observed at the top position of the head and the middle segment of the shell, while creep deformation is comparatively slight in the shell area that is next to the tube sheet. The results of simulation have indicated that, after the operation has proceeded for 10 hours, the maximum deformation that the heat exchanger can reach is 40 mm, and the maximum value of creep strain is 0.337; both two maximum numerical values were all recorded at the uppermost position of the head.

(4) For the usage in engineering, the simulation's output result can be changed into four maintenance index items: the stress-relaxation percentage, the biggest equivalent creep strain, the deformation-to-diameter proportion, and the hotspot migration route. In this current example, the 14.10 percent stress relaxation ratio and the 0.337 biggest creep strain show that the damage assessment ought to put emphasis on time-dependent strain building-up instead of only on the starting stress peak. In the process of service management, the transition part between head and cylinder ought to be given priority in fatigue-oriented nondestructive

examination, hence the head top region and middle shell region ought to be given priority in creep-deformation monitoring. This division of inspection objects is more effective than regarding the heat exchanger as one single homogeneous pressure vessel.

About the Author

Chen Yiwei was born in Zhejiang, China, in 1989. He received his master's degree from Zhejiang University and currently works in the Equipment Supervision Department of the Nuclear and Radiation Safety Center, Ministry of Ecology and Environment. His research focuses on mechanical analysis, vibration reduction, and noise reduction of nuclear power equipment.

Zhou Qiuhong was born in Hunan, China, in 1992. He received his bachelor's degree from Hunan University of Technology and currently works in the Equipment Supervision Department of the Nuclear and Radiation Safety Center, Ministry of Ecology and Environment. His research focuses on the informatization of nuclear power equipment.

Shi Hong was born in Hebei, China, in 1986 and holds a master's degree. He currently works in the Equipment Supervision Department of the Nuclear and Radiation Safety Center, Ministry of Ecology and Environment. His research focuses on seismic analysis and high-temperature creep analysis of nuclear power equipment.

Zhang Qiangsheng was born in Shanxi, China, in 1987. He received his master's degree from Tsinghua University and currently works in the Equipment Supervision Department of the Nuclear and Radiation Safety Center, Ministry of Ecology and Environment. His research focuses on seismic analysis and high-temperature creep analysis of nuclear power equipment.

Wei Dong was born in Shanxi, China, in 1986. He received his master's degree from Harbin Institute of Technology and currently works in the Equipment Supervision Department of the Nuclear and Radiation Safety Center, Ministry of Ecology and Environment. His research focuses on seismic analysis and high-temperature creep analysis of nuclear power equipment.

References

[1] Tang, L., Qian, H., Li, C., & Wu, X. (2023). Fretting fatigue test and simulation analysis of steam generator heat transfer tube. Metals, 13(1), 67.

[2] Li, Z., Wang, X., Wang, J., Lu, Y., & Shoji, T. (2020). High cycle fatigue behavior and numerical evaluation of Alloy 690TT steam generator tube. International Journal of Fatigue, 137, 105662.

[3] Xie, X., Peng, C., & Liang, Q. (2024). A cumulative damage model for tubes in nuclear power plants subject to continuous degradation and multi-effect shocks under dynamic environments. Annals of Nuclear Energy, 209, 110839.

[4] Xu, X., Xie, X., Liang, Q., & Peng, C. (2023). Probabilistic fracture mechanics analysis of heat transfer tube in floating nuclear power plant under multiple failure mechanisms. Nuclear Engineering and Design, 406, 112242.

[5] Jiang, Y., Xia, H., Zhang, J., Zhu, Y., Zhang, K., Huang, X., Yin, W., & Jiang, P. (2025). Digital twin model generation for crack propagation in steam generator tubes: Methods and implementation. Annals of Nuclear Energy, 224, 111697.

[6] ASME. (2025). ASME Boiler and Pressure Vessel Code, Section III: Rules for Construction of Nuclear Facility Components, Division 1. New York, NY: The American Society of Mechanical Engineers.

[7] Tubular Exchanger Manufacturers Association. (2019). Standards of the Tubular Exchanger Manufacturers Association (10th ed.). Tarrytown, NY: TEMA.

[8] International Atomic Energy Agency. (2023). Fatigue Assessment in Light Water Reactors for Long Term Operation: Good Practices and Lessons Learned (IAEA Nuclear Energy Series No. NR-T-3.32). Vienna: IAEA.

[9] Pernica, M., Letal, T., Losak, P., Nad, M., Reppich, M., & Jegla, Z. (2021). Transient thermal stress calculation of a shell and tube condenser with fixed tubesheet. Chemie Ingenieur Technik, 93(10), 1590-1597.

[10] Qi, K., Sun, H., & Lin, F. (2024). Finite element simulation of modal and linearized stress characteristics of key components of heat exchanger. Vibroengineering Procedia, 57, 112-118.

[11] European Committee for Standardization. (2017). EN 10028-2:2017 Flat Products Made of Steels for Pressure Purposes - Part 2: Non-alloy and Alloy Steels with Specified Elevated Temperature Properties. Brussels: CEN.

[12] Ansys, Inc. (2025). Ansys Mechanical APDL Theory Reference, Release 2025 R1. Canonsburg, PA: Ansys, Inc.

[13] ASME. (2019). Standard for Verification and Validation in Computational Solid Mechanics (ASME V&V 10-2019). New York, NY: The American Society of Mechanical Engineers.

[14] ASME. (2025). ASME Boiler and Pressure Vessel Code, Section III: Rules for Construction of Nuclear Facility Components, Division 5, High Temperature Reactors. New York, NY: The American Society of Mechanical Engineers.

[15] Koo, G.-H., Lee, S.-Y., Seo, J.-H., Song, K.-H., Choi, G.-S., & Sohn, M.-S. (2023). A study on creep-fatigue evaluation of nuclear cladded components by ASME-III Division 5. Energies, 16(6), 2898.

[16] Li, Z. H., Lu, Y. H., Hong, C., Zhao, Y. G., Han, Y. M., & Shoji, T. (2023). Corrosion fatigue damage mechanism and life evaluation of Inconel Alloy 690TT steam generator tube in high temperature pressurized water. Corrosion Science, 212, 110953.

[17] Li, Z. H., Lu, Y. H., You, L., Zhang, X. F., Wang, L., Tian, D. H., Zhang, W. D., & Shoji, T. (2024). Effect of temperature on corrosion fatigue behavior of Inconel Alloy 690TT steam generator tube. Corrosion Science, 227, 111741.

[18] Li, Z. H., Lu, Y. H., Hong, C., Zhao, Y. G., Zhang, W. D., & Shoji, T. (2023). Effects of foreign object damage on high-cycle fatigue behavior of Inconel Alloy 690TT steam generator tubes. Engineering Fracture Mechanics, 292, 109660.

[19] Moon, S., Kim, J.-M., Kwon, J.-Y., Lee, B.-S., Choi, K.-J., Kim, M.-C., & Han, S. (2022).

Modified theta projection model-based constant-stress creep curve for alloy 690 steam generator tube material. Nuclear Engineering and Technology, 54(3), 917-925.

[20] Lee, B.-S., Kim, J.-M., Kwon, J.-Y., Choi, K.-J., & Kim, M.-C. (2021). A practical power law creep modeling of alloy 690 SG tube materials. Nuclear Engineering and Technology, 53(9), 2953-2959.

[21] Kim, J.-M., Kim, M.-C., & Kwon, J.-Y. (2022). Evaluation of the creep rupture behavior of Alloy 690 steam generator tubes considering the pressure ramp rate. Journal of Pressure Vessel Technology, 144(1), 011504.

[22] Gustin, A. Z., Zuzek, B., & Podgornik, B. (2022). Creep life prediction of 10CrMo9-10 steel by Larson-Miller model. Materials, 15(13), 4431.

[23] Kopec, M., Brodecki, A., & Kowalewski, Z. L. (2023). Fatigue damage development in 10CrMo9-10 steel for power plant pipes in as-received state and after 280,000 h of exploitation. Archives of Civil and Mechanical Engineering, 23, 98.

[24] Majchrowicz, K., Romelczyk-Baishya, B., Wieczorek-Czarnocka, M., Marciniak, S., Mras, M., Kukla, D., Kopec, M., & Pakiela, Z. (2025). Assessment of 10CrMo9-10 power engineering steel degradation state by using small punch test. Materials, 18(17), 4133.

[25] Yang, Z., Dai, T., Yang, B., Wu, Y., Bai, Y., & Zhao, J. (2025). Creep life prediction of 10CrMo910 steel main steam pipes based on carbide evolution and machine learning. Materials Today Communications, 45, 112378.